# Cohesive modeling of ductile dynamic failure of pressurized metallic structures

O. R. van der Meulen[a,b,c,1], J. Mediavilla Varas[c], J. Weerheijm[c,d], and F. Soetens[a,b]

[a] *Eindhoven University of Technology, Faculty of Architecture, Building and Planning, Eindhoven, The Netherlands*
[b] *TNO Built Environment and Geosciences, Delft, The Netherlands*
[c] *TNO Defense, Security and Safety, Rijswijk, The Netherlands*
[d] *Delft University of Technology, Faculty of Civil Engineering and Geosciences, Delft, The Netherlands*

**Abstract**

Dynamic crack propagation of pressurized aluminum vessels has been studied. Rate insensitive cohesive zone models overpredict the rate of fracture. This was the motivation to implement a new Perzyna cohesive zone model, which is able to explain the low measured crack speeds.

## 1 Introduction

Fracture mechanics is used successfully to predict the progress of slow fracture processes as fatigue. Fast fracture of ductile materials, on the other hand, proves more difficult to predict accurately. This paper describes a series of tests on aluminium pressure vessels, representing airplane fuselages and a new rate sensitive cohesive zone model to model these.

Accurate estimations of the rate of fracture are of particular interest to the oil and gas industry. Uncontrolled pipeline failure may fail to arrest for many kilometers, if the fracture speed exceeds the gas depressurization speed. Industry formulas to determine the potential for this to occur exist, but are based on empirical measurements and need to be validated for higher strength steels [1].

Another field of application is the research on the severity of occurrences of boiling liquid expanding vapor explosions, also known as BLEVE [2]. In road vehicles carrying liquefied gasses at pressure, a notch resulting from some accident may cause complete containment failure in a matter of milliseconds, leaving the liquefied gas in an unstable superheated state, which then regasifies almost instantaneous, equivalent to a powerful explosion. The severity and even the very occurrence, of a BLEVE are controlled for a great part by the fracture propagation rate.

### 1.1 Analytical boundaries to the speed of fracture

Analytical boundaries to the speed of fracture do exist, and it is generally accepted that the Rayleigh wave speed serves as an absolute upper bound [3]:

$$c_R = c_S \frac{0.862 + 1.14\nu}{1 + \nu}. \tag{1}$$

where,

$$c_S = \sqrt{\frac{E}{2\rho\,(1+\nu)}}. \tag{2}$$

[1] Corresponding author
*Email address:* o.r.v.d.meulen@tue.nl

This yields an upper bound for steel and aluminum of 3000 and 2800 $m/s$ respectively. Attempts to lower the upper bound fracture propagation rate by using the Griffith model have resulted in an asymptotic upper bound for brittle fracture and fracture lengths orders greater then the initial crack length [4]:

$$c_{\text{limit}} = 0.38c_0. \tag{3}$$

where $C_0$ is the material sound speed:

$$C_0 = \sqrt{\frac{\mu}{\rho}}. \tag{4}$$

This lowers the upper bound to fracture speeds of 2000 $m/s$ for steel and 1900 $m/s$ for aluminum. This is still many times faster than the speeds observed in experiments, which lie in the range of 300 - 500 $m/s$ [5].

## 2 Experiments on pressurized barrels

The EU VULCAN projects aims at studying the vulnerability of airplane fuselages in case of an internal explosion and fire. In this framework, tests were carried out at TNO DSS[2] on pressurized aluminum 2024 T3 barrels to obtain the speed of fracture in airplane fuselages. The dimensions and internal pressures of the barrels are given in Table 2. High speed cameras were used to monitor the fracture propagation. Fracture was triggered with the use of explosives and a static anvil bar, creating an initial notch in shear of length $2a$. figure 1a shows a post mortem of the test setup. figure 1b shows the fracture surface of another test performed on the same batch of one millimeter thick aluminum, indicating ductile failure through void coalescence as the fracture mechanism. The recorded fracture speeds were less than 300 $m/s$ (see later figure 6 and Figure 7).

| Test | Pressure $kPa$ | 2a $mm$ | Height $mm$ | Diameter $mm$ | Thickness $mm$ |
|---|---|---|---|---|---|
| Test02alu1 | 310 | 280 | 1030 | 1200 | 1 |
| Test03alu2 | 230 | 200 | 1030 | 1200 | 1 |

Table 1: Test barrel geometry and load.

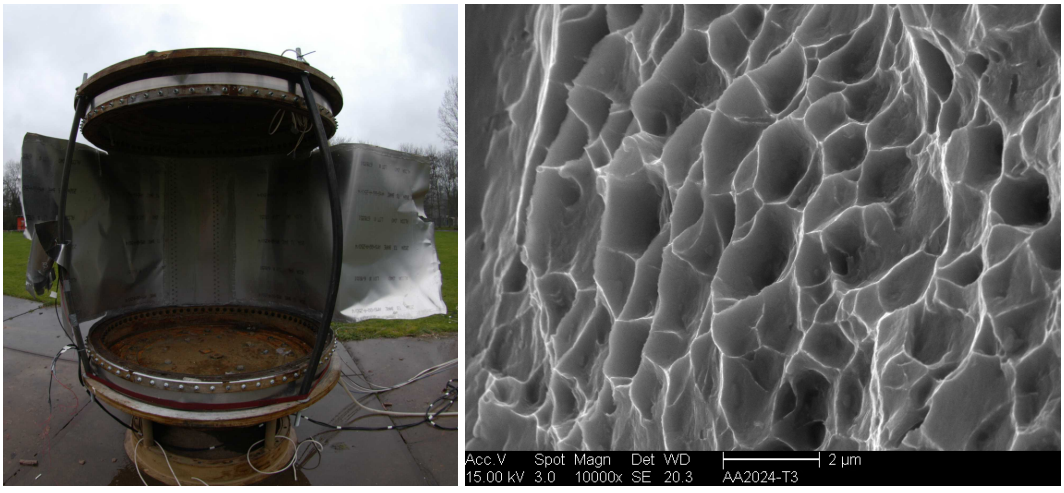


(a) Barrel test after fracture

(b) Close-up of fracture surface.

Figure 1: The results of fracture

[2]TNO Defense, Security and Safety, Rijswijk, The Netherlands

# 3 Shortcomings of standard CZ models for dynamic crack propagation

To predict the dynamic crack behavior of the pressurized barrels described in section 2, the nonlinear explicit finite element code LS-DYNA has been used. Explicit finite element codes are especially well suited for highly transient phenomenon as fast fracture. Fracture is modeled by means of the *cohesive zone* (CZ) approach. The cohesive zone serves to incorporate all nonlinearities in the fracture process zone in a single row of elements of negligible width. Cohesive zones are used as intermediate elements in between two bulk meshes and define a possible fracture path. The cohesive behavior is defined by a cohesive energy $\Gamma$, a maximum traction $T$, and a non-dimensional traction separation law or TSL. The maximum traction and cohesive energy are not independent from one another and need to be obtained together [6]. Figure 2 depicts the type of TSL used in this research. The cohesive properties of aluminum

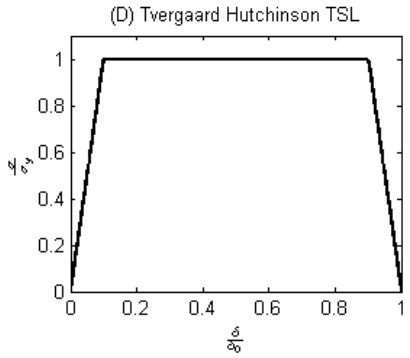


Figure 2: CZ law model with a tri-linear traction-separation law

2024 T3 were obtained from reference [7], where an inverse modeling technique was applied to a centre cracked tension test, with a similar thickness as that of our barrel tests. A cohesive energy $\Gamma = 18\ N/mm$ and a maximum traction of $T = 2.1\sigma_y$, with $\sigma_y$ being the material yield stress. This value is comparable to the value reported in [8, 9] of $\Gamma = 17$ - $19\ N/mm$, and $T = 2$ - $2.7\sigma_y$.

Using these cohesive properties to do simulations of the barrel experiments of section 2, leads to a gross overestimation of the actual fracture speed, roughly $c = 1100\ m/s$, instead of the $300\ m/s$ measured. See figure 3. To reproduce the test data, a significantly higher cohesive energy is needed, $\Gamma = 100\ N/mm$. This indicates than in dynamic fracture the cohesive energy must be higher than in the static case. Nevertheless, no experimental data on the fracture energy at high rates was available to confirm these findings.

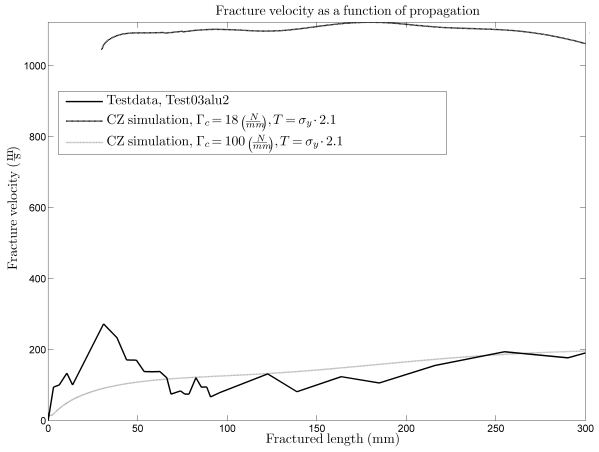


Figure 3: Test data with regular and increased cohesive energy level simulations.

# 4 Motivation for using a rate dependent cohesive zone model

During dynamic crack propagation, the material undergoes rapid strain rate changes. As many mechanical properties, the fracture energy is also rate sensitive. Thus using one constant static fracture energy during dynamic crack propagation is not realistic. We believe this rate sensitivity is partly responsible for the discrepancies in crack speed between experiments and conventional (non-strain rate sensitive) cohesive zone models. This is the motivation of the work presented in this paper. A user defined rate sensitive cohesive zone model has been developed in LS-DYNA, namely a visco-plastic Perzyna type cohesive model.

## 4.1 Constitutive equations

The continuum Perzyna model was adapted for use in cohesive zones and is defined by the following set of partial differential equations. Note that work hardening has been excluded. The variable $\hat{t}$ denotes a traction (3 components), not a stress tensor (9 components).

$$\psi(\hat{t}_{eq}) = \left\langle \frac{\hat{t}_{eq}}{T} - 1 \right\rangle^{N_{\text{pz}}}. \tag{5}$$

$$\dot{\boldsymbol{\delta}}_{\boldsymbol{vp}} = \frac{1}{\eta}\psi(\hat{t}_{eq})\frac{\partial \hat{t}_{eq}}{\partial \hat{\boldsymbol{t}}}. \tag{6}$$

$$\dot{\hat{\boldsymbol{t}}}_{\boldsymbol{el}} = \dot{\hat{\boldsymbol{t}}} - \dot{\hat{\boldsymbol{t}}}_{\boldsymbol{vp}} = K(\dot{\boldsymbol{\delta}} - \dot{\boldsymbol{\delta}}_{\boldsymbol{vp}}). \tag{7}$$

This system of differential equation is numerically integrated using a simple Euler forward type integration. First the equivalent traction is calculated:

$$\hat{t}_{eq,n} = T\sqrt{\frac{\hat{t}^2_{\text{III},n-1}}{S^2} + \frac{\hat{t}^2_{\text{II},n-1}}{S^2} + \frac{\hat{t}^2_{\text{I},n-1}}{T^2}}. \tag{8}$$

And then the overstress function:

$$\psi_n(\hat{t}_{eq}) = \left\langle \frac{\hat{t}_{eq,n}}{T} - 1 \right\rangle^{N_{\text{pz}}}. \tag{9}$$

Followed by the normal to the yield surface:

$$\begin{aligned}
\frac{\partial \hat{t}_{eq,n}}{\partial \hat{t}_{\text{III},n-1}} &= \frac{T\hat{t}_{\text{III},n-1}}{S^2\sqrt{\frac{\hat{t}^2_{\text{III},n-1}}{S^2} + \frac{\hat{t}^2_{\text{II},n-1}}{S^2} + \frac{\hat{t}^2_{\text{I},n-1}}{T^2}}}, \\
\frac{\partial \hat{t}_{eq,n}}{\partial \hat{t}_{\text{II},n-1}} &= \frac{T\hat{t}_{\text{II},n-1}}{S^2\sqrt{\frac{\hat{t}^2_{\text{III},n-1}}{S^2} + \frac{\hat{t}^2_{\text{II},n-1}}{S^2} + \frac{\hat{t}^2_{\text{I},n-1}}{T^2}}}, \\
\frac{\partial \hat{t}_{eq,n}}{\partial \hat{t}_{\text{I},n-1}} &= \frac{\hat{t}_{\text{I},n-1}}{T\sqrt{\frac{\hat{t}^2_{\text{III},n-1}}{S^2} + \frac{\hat{t}^2_{\text{II},n-1}}{S^2} + \frac{\hat{t}^2_{\text{I},n-1}}{T^2}}}.
\end{aligned} \tag{10}$$

And the plastic part of the opening rate:

$$\dot{\boldsymbol{\delta}}_{\boldsymbol{vp,n}} = \frac{1}{\eta}\psi_n\left(\hat{t}_{eq,n}\right) \cdot \frac{\partial \hat{t}_{eq,n}}{\partial \hat{\boldsymbol{t}}_{\boldsymbol{n-1}}}. \tag{11}$$

Finally the traction update is computed:

$$\hat{t}_{\text{II,III},n} = \hat{t}_{\text{II,III},n-1} + K_1\left(\dot{\delta}_{\text{II,III},n} - \dot{\delta}_{vp,\text{II,III},n}\right)\Delta t. \tag{12}$$

An additional penalty term is included for normal compression forces to avoid penetration:

$$\hat{t}_{\mathrm{I},n} = \begin{cases} \hat{t}_{\mathrm{I},n} + K_1(\dot{\delta}_{\mathrm{I},n-1} - \dot{\delta}_{vp,\mathrm{I},n})\Delta t & \text{, Without penalty} \\ \hat{t}_{\mathrm{I},n} + K_1(\dot{\delta}_{\mathrm{I},n-1} - \dot{\delta}_{vp,\mathrm{I},n})C_{\mathrm{pen}}\Delta t & \text{, With penalty} \end{cases} \tag{13}$$

with $K_1$ being the elastic stiffness of the cohesive zone.

The maximum opening is independent of the opening rate and can be calculated from the cohesive energy, the shape of the TSL and the maximum traction. To calculate the maximum combined opening, a power law equation is used:

$$\delta_{0,n} = \frac{1+\beta_n^2}{\mathrm{A_{N.TSL}}} \frac{1}{\sqrt[\mathrm{XMU}]{\left(\frac{T}{\Gamma_{\mathrm{N}}}\right)^{\mathrm{XMU}} + \left(\frac{S\beta_n^2}{\Gamma_{\mathrm{T}}}\right)^{\mathrm{XMU}}}}. \tag{14}$$

where $A_{\mathrm{N.TSL}}$ is the area under the normalized TSL and $\beta$ is the "mode mixity", expressing a ratio between normal and tangential opening:

$$\beta_n = \frac{\sqrt{\hat{\delta}_{\mathrm{II},n} + \hat{\delta}_{\mathrm{III},n}}}{\delta_{\mathrm{I},n}}. \tag{15}$$

The current combined opening is expressed as:

$$\delta_{\mathrm{eq},n} = \sqrt{\hat{\delta}_{\mathrm{III},n} + \hat{\delta}_{\mathrm{II},n} + \langle\delta_{\mathrm{I},n}\rangle}. \tag{16}$$

The normal opening $\delta_I$ is enclosed by McCauley brackets to exclude compressive forces. The tangential opening directions are integrated according to:

$$\hat{\delta}_{\mathrm{II,III}} = \int \dot{\delta}_{\mathrm{II,III}}\Delta t \cdot \mathrm{sign}\left(\sigma_{\mathrm{II,III}}\right). \tag{17}$$

The declining stress part of the cohesive zone model is described by a damage opening distance $\delta_{\mathrm{dam}}$. At each time step, the sum of the current opening $\delta_{\mathrm{eq}}$ and the damage opening distance $\delta_{\mathrm{dam}}$, is checked against the maximum opening $\delta_0$. When this is exceeded, the element is no longer governed by the visco-plastic system of equations, but rather by a linear damage formulation. As can be seen in figure 5, the failure opening is equal for all opening rates.

## 4.2 Gauss point tests

The opening rate dependent cohesive zone model described in section 4.1 has been tested at single gauss point level. this is shown in figure 4. The maximum traction $T$ and the fracture energy $\Gamma$ (the area below the $\hat{t}$ - $\delta$ curve) increases with the opening rate, while leaving the maximum opening unchanged. This causes the cohesive energy to rise and bring the speed of fracture down.

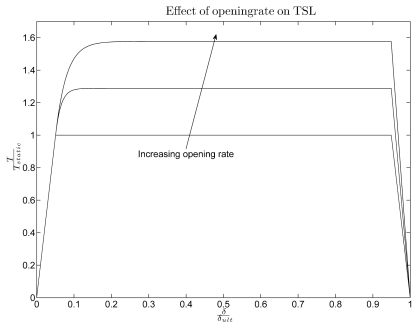


Figure 4: Perzyna cohesive zone model. an increase in the maximum traction and fracture energy is observed at increasing opening rates.

Another interesting feature of the Perzyna model is that it is able to cope with discontinuities in opening rate, while returning a continuous stress response. This can be observed from figure 5.

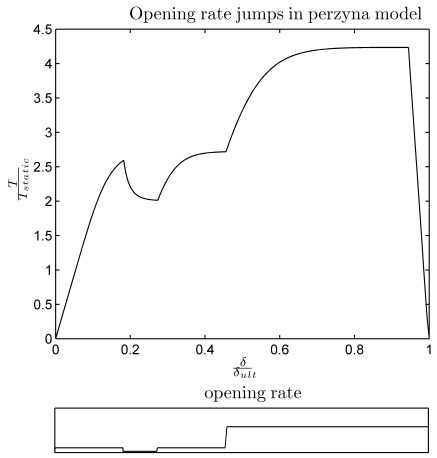


Figure 5: Perzyna type cohesive zone's response to a discontinuous opening rate.

## 4.3 Parameter determination

The Perzyna cohesive zone model has two additional parameters as compared to standard cohesive zone formulations, i.e. the apparent viscosity $\eta$ and the Perzyna exponent $N_{\text{pz}}$, which need to be obtained.

The two tests with pressurized barrels [10] served as the basis for this. From one of the tests, "Test03alu2", depicted in figure 6, we were able to estimate the Perzyna parameters $\eta = 0.315$ and the Perzyna exponent $N_{\text{pz}} = 2.875$. For comparison, a simulation with a standard cohesive zone with identical cohesive properties is also included. The differences in crack speed of the two models are very large.

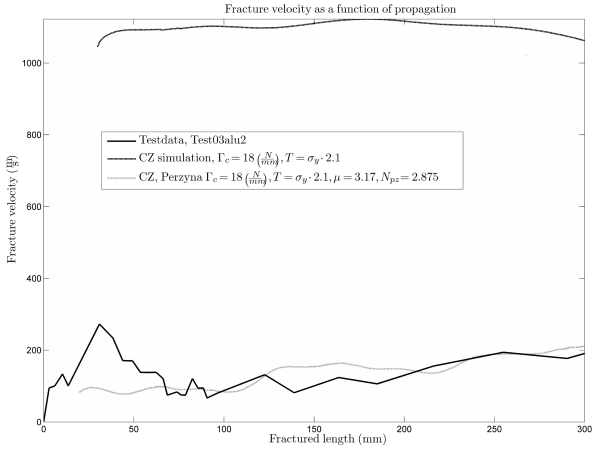


Figure 6: Custom cohesive zone model trained by experimental data.

## 4.4 Model validation

The visco-plastic Perzyna parameters obtained in 4.3 were used to do a simulation of the second barrel test. The results of which are presented in figure 7. The experimental data curve seems to converge to the fracture speed values obtained with the newly developed visco-plastic cohesive zone model. Unfortunately, the experimental data set is far from complete; the fracture ran outside the scope of the recording high speed cameras.

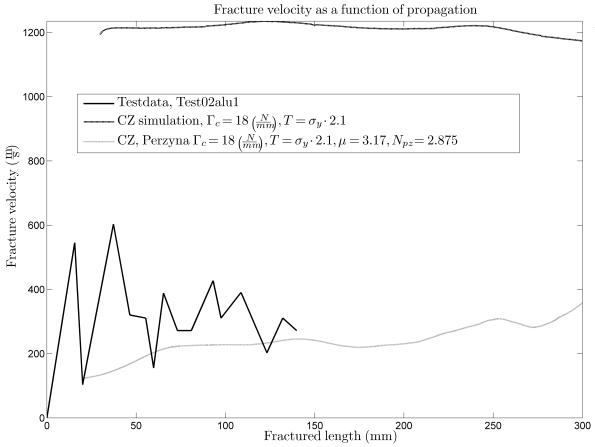


Figure 7: Testing the custom cohesive zone model against experimental data.

The difference in initial velocity of the tests and the simulations may be explained by the method of initiation. Both barrel test fractures were started with the help of explosives, the simulations however, were started using a set of constraints, holding an initial notch closed until the designated time of failure. At that time a bulge started forming, allowing the fracture to speed up as it is formed. The explosive charge not only created the required bulge almost instantaneous, it would have also imparted kinetic energy to the material surrounding the fracture. This explains the initial peak in fracture propagation rates.

# 5 Future work

Recently an new tests series was performed on barrels made out of aluminium 2024 T3, Glare 3 3/2 0.4, and CFRP composite to compare their relevant performance as an airplane fuselage material in cases of internal explosions. Figure 8 shows the preliminary test results. Additional results are presented at ICF12 and in [11].

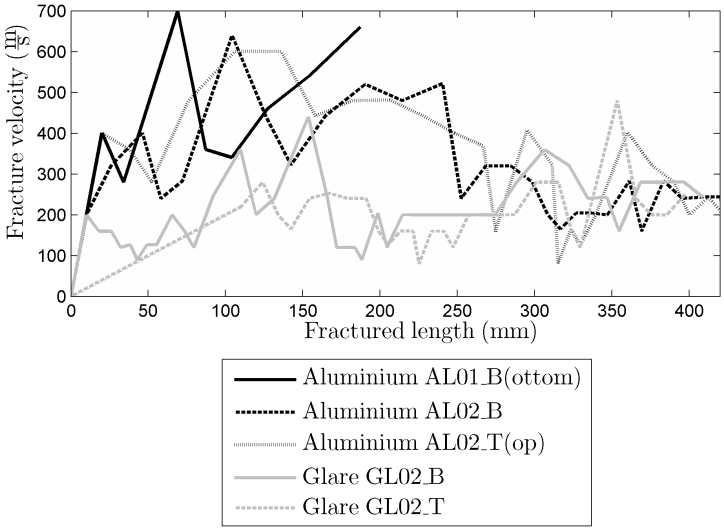


Figure 8: Barrel with an initial notch $2a = 56\ mm$ and an internal pressure of 200 $kPa$ subjected to an internal explosion equivalent to 54 grammes of TNT.

# 6 Conclusions

Two tests on pressurized aluminum barrels made out of 2024 T3 were performed. Using conventional cohesive zone formulations and the static cohesive energy level, we were unable to reproduce the experimental fracture propagation rates. Reproducing the observed fracture speed required cohesive energy levels as much as five times as high. A visco-plastic, opening rate sensitive CZ model has been developed for LS-DYNA. The new visco-plastic CZ model accurately predicts the stable fracture propagation rates in barrel tests made of aluminum 2024 temper T3.


# acknowledgements

The authors wish to express their gratitude to the EU VULCAN project, for its financial support.

# References


[1] G. Demofonti, G. Mannucci, C.M. Spinelly, L. Barantsi, and H.G. Hillenbrand. Large-diameter x100 gas line pipes: Fracture propagnation evaluation by full-scale burst test. Technical report, Europipe, 2000.

[2] A.C. van den Berg, M.M. van der Voort, J. Weerheijm, and N.H.A. Versloot. Bleve blast by expansion-controlled evaporation. *Process Safety Progress*, 25:44–51, 2005.

[3] D. Sherman. Macroscopic and microscopic examination of the relationship between crack velocity and path and rayleigh surface wave speed in single crystal silicon. *Journal of the Mechanics and Physics of Solids*, 53(12):2742–2757, December 2005.

[4] D. Hull and P. Beardmore. Velocity of propagation of cleavage cracks in tungsten. *International Journal of Fracture*, 2(2):468–487, June 1966.

[5] J. Mediavilla, J. van Deursen, and J. Weerheijm. Mechanical aspects of the initiation of a bleve. Technical report, TNO Defence, Security and Safety, 2008.

[6] W. Brocks. Ductile crack extension in thin-walled structures six lectures cism course "nonlinear fracture mechanics models". Technical report, GKSS Research Centre, Geesthacht, July 2008.

[7] T.J. de Vries and C.A.J.R. Vermeeren. R-curve testdata: 2024-t3, 7075-t6, glare 2 and glare 3. Technical report, TU-Delft, 1995. LR M-705.

[8] Sushovan Roychowdhury, Yamuna Das, Arun Roy, Robert H, and Dodds. Ductile tearing in thin aluminum panels: experiments and analyses using large-displacement, 3-d surface cohesive elements. *Engineering Fracture Mechanics*, 69:983–1002, 2002.

[9] W. Brocks and Th. Siegmund. Effects of geometry and material on the energy dissipation rate. In M. Fuentes, M. Elices, A. Martn Meizoso, and J. M. Martnez-Esnaola, editors, *Fracture Mechanics: Applications and Challenges : Invited Papers Presented at the 13th European Conference on Fracture*, San Sebastian, September 2000. ECF, Elsevier.

[10] Jesus Mediavilla, Jaap Weerheijm, Ronald van der Meulen, F. Soetens, C. Wentze, and J. van Deursen. Dynamic crack propagation: an experimental-numerical approach. In J. Pokluda, P. Lukáš, P. Sandera, and I. DLouhý, editors, *17th European Conference on Fracture. Book of Abstracts and Proceedings on CD ROM*, pages 2039–2046, 2008.

[11] J. Mediavilla, F. Soetens, O. R. van der Meulen, and M. Sagimon. Dynamic crack propagation of glare and cfrp fuselage materials. In *Proceedings of: Deformation and Fracture of Composites Conference (DFC10)*, Sheffield United kingdom, April 2009. Sheffield University.